Chapter 7

CuO assisted 1393B3 on in vitro biological and mechanochemical performance, and in vivo bone healing potential in rat bone defect model

7.1 INTRODUCTION

Glasses are known for their likelihood to avoid crystallization during cooling from viscous melts. B_2O_3 in borate glasses is the glass network former like SiO_2 in silicate glasses. While both being network formers, they differ by their viscosity (as melt) and crystallization tendency. Borate glasses have relatively facile viscous flow behavior than silicate glasses at liquidus temperature; therefore, they have a higher devitrification tendency than that of the silicate glasses (Schmelzer et al., 2005).

However, bioactive glasses are different from conventional glasses by their composition, properties, and applications. Bioactive glasses was first coined in the late 1960s by Prof. Lary L. Hench. Since then, bioactive glasses/ scaffolds have triggered a revolution in tissue engineering applications. The bioactivity of such glasses is the ability to elicit a specific response from the host tissue to form a material-tissue compliant strong bond at the interface (Ali et al., 2018, Ali et al., 2020b).

However, the traditional glass network former SiO_2 from 1393 glass is completely replaced by B2O3 in 1393B3 glasses (Rahaman et al., 2011). The typical chemical composition of 1393B3 is B_2O_3-56.6%, CaO-18.5%, Na_2O-5.5%, MgO-4.6%, K_2O-11.1%, P_2O_5-3.7% (wt. %). The 1393B3 glass follows the reaction kinetics of 45S5 and converts to glass-ceramics when sintered (Fu, 2009). Unlike the silicate based 1393, the borate 1393B3 cannot be easily drawn to glass fibers and form scaffolds until it is converted to crypto-crystalline

form by means of control heat treatment (Jung and Day, 2009). Borate based bioactive glasses due to their faster degradation, and thereby faster reaction and subsequent conversion to bone minerals (HA; $Ca_{10}(PO_4)_6(OH)_2$) are considered favorable for tissue engineering (TE) application (Rahaman et al., 2011, Huang et al., 2006).

The 1393B3 glasses convert to bone minerals faster and more efficiently than 1393 and leave no leftover of silica-rich layer like silicate glasses (Bi et al., 2013, Huang et al., 2006, Yao et al., 2007). Further, the conversion of HA is claimed to be controllable easily in borate glasses than the silicate glasses.

However, boron is another important trace elements like zinc and iron that involves in building healthy bones. Boron is also responsible for improving brain electrical signaling and wound healing ability and prevents short-term memory loss for the elderly (Pizzorno, 2015). Moreover, boron itself is a therapeutic ion and used to treat certain tumors and cancers and their presence in bioactive glasses, therefore introduces the therapeutic properties like bone and wound healing by osteogenesis and angiogenesis (Xia et al., 2019, Barth et al., 1990).

However, the introduction of copper into the bioactive glass was previously studied by researchers for the betterment of mechanical properties, wound healing ability, and neovascularization (Ali et al., 2018, Kargozar et al., 2018, Finney et al., 2009, Gérard et al., 2010). Further, copper deficiency has been reported to have suppressed the new blood vessel formation (Raju et al., 1982). Copper was also reported as an osteogenic stimulant in the mesenchymal stem cells and osteoblastic cells (Wu et al., 2013). Nevertheless, there is a limit up to which copper is therapeutic and non-toxic, and beyond that limit, copper is toxic. However, the permissible limit of CuO in bioactive glass in two separate

investigations were reported to 0.8 % and 3.0 % (wt%), respectively (Lin et al., 2016, Wang et al., 2014). Moreover, we also observed an insignificant cytotoxicity or maximum cellular viability up to 2.0 %. CuO incorporation into the 1393 glass scaffolds.

Herein, the CuO incorporated 1393B3 glass along with the parent glass system (pure 1393B3) has been examined to analyze their in vitro biological and mechanochemical performance. The in vivo bone regeneration potentiality of the scaffolds was studied by the bone defects model in Wister rats.

7.2 MATERIALS AND METHODS

7.2.1 Scaffolds preparation

The glasses were melted in a control heating electric furnace at 1250±10 ˚C using Pt. crucibles. Prior melting, the glass batches were prepared by mixing proportionate amounts of raw materials in agate mortars for at least 30 min. The reagents used in preparing the BBG and CBBGs (Table 7.1) were AR grade carbonates of sodium, calcium, potassium and magnesium, boric acid, ammonium dihydrogen orthophosphate, and cupric oxide (Assay: 98–99.9%, Loba chemie, Mumbai, India). The glass melts were immediately quenched in double distilled (Millipore) water. Then the glass batches were dried and crushed and ground manually using agate mortar. The glass powder was ball milled in liquid medium (ethanol) using Al_2O_3 balls for an additional 2- 4 h in a 15 min cycle. Then a slurry was prepared for each glass powder by mixing ‘powder: water (double distilled): ethanol’ in the ratio of 2:2:1. PVA solution was prepared and added to the slurry by 5.0 wt % of the powder. The slurry was kept on stirring on a magnetic stirrer (Spinot, Tarsons digital, IN) for additional 2-4 h prior PU foams of required dimensions (25×10×10 mm and 10×10×10 mm) were soaked for slurry impregnation. The additional slurry was injected

from the top of the foams to evenly coat the surface. The slurry infiltrated foams were kept on drying at 80 ˚C for half an hour. The excess slurry was then removed from the surface, and the foams were dried at 120 ˚C for two days. Then, the foams were provided with control heat treatment (sintering) to convert the glasses into crystals (glass-ceramic) at 700-750 ˚C. Finally, the 3D porous scaffolds (BBG and CBBGs) were developed.

Table 7.1: Chemical composition of 1393B3 glass in mole%

Code (Scaffolds)	SiO_2	CaO	Na_2O	K_2O	MgO	P_2O_5	CuO
BBG (1393B3)	54.6	22.1	6	7.9	7.7	1.7	0
C1BBG (1393B3-0.5% CuO)	54.1	22.1	6	7.9	7.7	1.7	0.5
C2BBG (1393B3-1.0% CuO)	51.6	22.1	6	7.9	7.7	1.7	1
C3BBG (1393B3-2.0% CuO)	52.6	22.1	6	7.9	7.7	1.7	2

7.2.2 Methods

The *in vitro* bioactivity of BBGs was examined by immersing the samples in SBF for particular days. Methods (XRD, FTIR, SEM-EDX, and pH of the SBF solution) used in determination of bioactivity of BBGs were described in chapter 4 and chapter 6.

7.2.3 Biological compatibility of BBGs using L929 cell lines

Biological compatibility of our derived scaffolds was assessed using mouse fibroblast L929 cells. The L929 cell lines purchased from NCCS (National Center for Cell Science, INDIA) were used to determine the cell survivability and proliferation by LIVE/DEAD assay and cellular metabolism in the glass environment (BBG and CBBGs). The purchased cell lines

upon receiving kept for culturing immediately in complete cell culture medium supplemented with 10% fetal bovine serum (FBS) and 100 U/ml penicillin-streptomycin at 37 ˚C in 95% humidified, 5% CO_2 atmosphere.

Cell confluence upon attaining to 70%, the cell culture plates were trypsinized (0.25%) in 95% humidified, 5% CO_2 atmosphere at 37 ˚C. The trypsinized cells after centrifugation at 300g for 10 min were re-suspended. The pellets were washed with PBS twice. Glass scaffolds (BBG and CBBGs), prior using for cell culture were prepared by sterilizing with ethanol/UV and were subsequently incubated in complete culture media for 2h at 37 ˚C in 95% humidified, 5% CO_2 environment. Biological compatibility of the scaffolds was then assessed by using the L929 cell lines.

Viability of L929 cells in the derived scaffolds by LIVE/DEAD assay was assessed by using Calcein AM and Ethidium homodimer-1 staining. Cellular metabolic activity of the L929 cells in the BBGs were evaluated by MTT (3-(4, 5-dimethylthiazol-2-yl)-2, 5-diphenyltetrazolium bromide) assay. The cell-scaffold interactions by means of cellular attachments onto glass surfaces were assessed by obtaining the microscopic images of the cell adhesion from the scanning electron microscope (SEM) EVO|18 (ZEISS, US) to examine biological compatibility of the developed scaffolds. The BBG and CBBG scaffolds after being seeded with cell (L929) suspension of 1×10^5 cells / cm^2 were cultured for a particular period in 95 % humidified, 5 % CO_2 atmosphere at 37 ˚C. The scaffolds on an interval washed with phosphate-buffered saline (PBS) and incubated for 2 h along with 100 µl of fresh complete media and 10 µl of MTT reagent (5 mg/ml). Afterward, the formazan crystals were solubilized by mixing with 100 µl of solubilization solution. Cellular metabolism in the BBGs was then measured by taking the absorbance at 570 nm.

Likewise, cells' viability after grown onto scaffolds for 24 h and subsequent incubation for 30-40 min in Calcein AM and Ethidium homodimer-1 staining solution was visually inspected. The viable (green) and dead (red) cells were identified using Olympus BX51 fluorescence microscopy (Japan).

7.2.4 Evaluation of mechanochemical performance of porous BBGs

The mechanical properties of the scaffolds were evaluated using universal testing machine (UTM) H10KL (Tinius olsen, US), maintaining 0.05mm/min crosshead speed under 10 KN load cell. Mechanical properties (compression and 3 point bending) of the samples with required dimension in both dry (sintered only) and wet (at 15 days of soaking) conditions were assessed to validate their mechanical stability in physiological liquid. The flexural strengths of our porous glass scaffolds were measured in accordance with the standard protocol ASTM C1674-11. The bending modulus (or flexural modulus) was derived from the stress strain diagram.

Apparent porosities of BBG and CBBGs were measured in accordance with ASTM C20-00 via solvent saturation method by boiling water. The % P (porosity) was calculated by the ratio of volume of the open pores (V_{op}) to the exterior volume of the scaffolds (V) solvent as follows:

$$\% \, P = \frac{V_{op}}{V} \times 100$$

Where $V_{op} = W_{soaked} - W_{dry}$ and $V = W_{soaked} - W_{suspended}$ (W is weight of scaffolds in air and soaked and suspended in water).

Hence,

$$\% \, P = \frac{W_{soaked} - W_{dry}}{W_{soaked} - W_{suspended}} \times 100$$

The degradability of bioactive glasses are their ability to degrade and convert to bone minerals (HA) in physiological liquid. Here, the degradability of the scaffolds were assessed by weight loss which is also associated with chemical durability of glasses (Wang et al., 2014). Chemical durability of glasses is the measure of resistance that they provide towards chemical attack (Ali et al., 2018). Biodegradability (degradation in biological fluid i.e. SBF), thus, in another sense is reciprocal to the chemical durability. Most biodegradable glass is therefore, least chemically durable.

$$\% \text{ Weight loss } = \frac{W_i - W_f}{W_i} \times 100$$

Where W_i=initial weight; W_f=final weight

7.2.5 The in vivo studies

7.2.5.1 Animals' surgical operation

Albino-Wister rats of 200-250 g of both sexes were purchased from Animal House, IMS, BHU, Varanasi. The rats were acclimatized for at least 2 weeks in the animal facility before

surgical operations. Nine rats were grouped into three i.e. (i) Gr A (control/blank-bone defects created and left untreated), (ii) Gr B (BBG test group-bone defects created and treated with BBG) and (iii) Gr C (CBBG test group-bone defects created and treated with the best of CBBGs) consisting three rats in each group. The defects (length ~4mm, width ~2mm) in the femoral bones were created using a high precision dental drill after anesthetizing the animals with Thiopental sodium (20 mg/kg body weight) followed by saline irrigation. The 'Gr B' and 'Gr C' animals were filled the defect sites with BBG and C2BBG (considering best in CBBGs in terms of in vitro tests), while 'Gr A' left untreated. The animals were provided with ad libitum food and water throughout the study until sacrificed (36^{th} day). After 5 weeks of constant monitoring, the rats were sacrificed on 36^{th} day following the central animal ethical committee's protocol (Protocol No. Dean/2015/CAEC/1421).

7.2.5.2 Radiological examination of defects

Bone defects remodeling by neo bone formation and healing of wounded sites of animals were assessed through radiographs on day1 and day35 of post-surgical operations.

7.2.5.3 Histology

The rats were sacrificed, and the femur bones were collected. The bones were washed, and stored in 10% formalin up to one week. The bone specimen after decalcification with 10% EDTA were cut into 6 μm sections, and stained with Haemotoxylin and Eosin (H&E). The stained sections were subjected to Olympus BX51 microscope (Japan) to examine the formation of new bones/ connective tissues in the defect area.

7.2.5.4 Renal function tests (RFTs), lever function tests (LFTs) and alkaline phosphatase (ALPase) of blood serum

First of all, blood was collected directly from the heart of the anesthetized animals. Then, the blood serums from the blood were separated by centrifugation, and stored at <40 ˚C. Blood serums were investigated for assessment of change of different biochemical parameters responsible for bone related health anomalies. The biochemical parameters include ALT (Alanine Aminotransferase), ALP (Alkaline Phosphatase), Urea, and Creatinine were assessed in this investigation.

7.3 Statistical analysis

Statistical analysis by one way ANOVA followed by Tukey's post hoc test was performed while comparing differences between groups. Experiments were performed in triplicates and the data were expressed as mean ± standard deviation (SD). Differences were considered significant for 'p' < 0.05 (*) and highly significant for 'p' < 0.01(**) and 0.001(***).

7.4 RESULTS

7.4.1 The in vitro bioactivity assessment via structural, functional, morphological and physico-chemical investigation

BBG and CBBGs were evaluated for bioactivity after 15 days of immersion in SBF. Fig 7.1 illustrates X-ray diffractogram of the sintered only (bottom four curves) and SBF treated (top four curves) scaffolds. Herein, the structural characterizations of the glass samples by XRD clearly demonstrate fundamental alterations in peaks characteristic in soaked samples in comparison to sintered only scaffolds.

Here, we observed some obviously pronounced peaks in SBF treated scaffolds, particularly at the angular value (2θ) 32˚, 45˚, and 56˚. Surprisingly, the peak intensities in CBBGs for the SBF treated samples were also found to be enhanced with the increase in CuO percent in 1393B3.

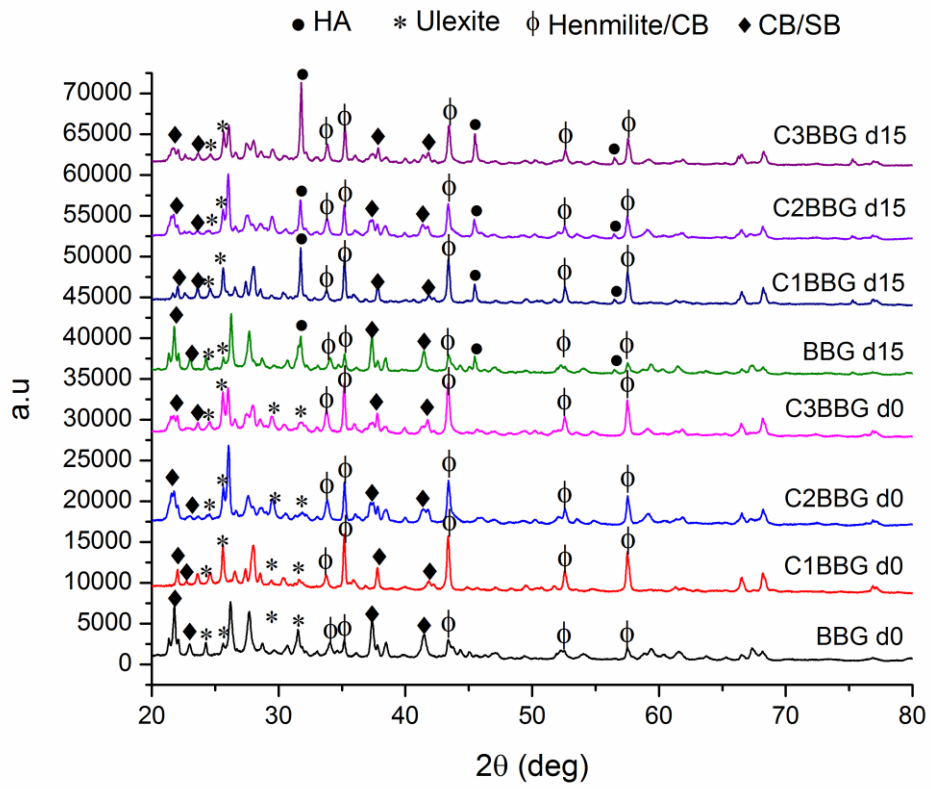

Fig 7.1 XRD of BBGs 'soaked for 15days in SBF' (above 4 curves) and sintered only (below 4 curves) samples. Characteristics peaks show HCA layer formation for soaked samples.

Further, the vibrational bands of FTIR spectra were analyzed to identify the molecular functional groups present in the glass samples. Bending vibrations that occur at lower frequencies were noticed at 400-700 cm^{-1}. Fig 7.2 reports the spectral vibrations of various functional groups of phases within IR region (4000 to 400 cm^{-1}). Characteristics IR

spectrums indicating fundamental variations in resonant frequencies were noticed within 400 cm^{-1} to 1200 cm^{-1}. The results demonstrate that the characteristics spectrum in pre-SBF treated samples were altered considerably after 15 days of immersion in SBF. The main characteristics bands in sintered only samples were explicitly noticed at 420, 455, 520, 560, 604, 645, 750, 1000, 1020, and 1095 cm^{-1}. However, the appearance of new vibrational resonances in the IR spectrum of soaked samples were observed at 410, 422, 434, 460, 474, 490, 500, 518, 528, 562,588, 598, 618, 644, 660, 674, 750, and 1035 cm^{-1}. The vibrational bands at higher frequencies (not shown) were observed at 2800-3700 cm^{-1} correspond to OH groups.

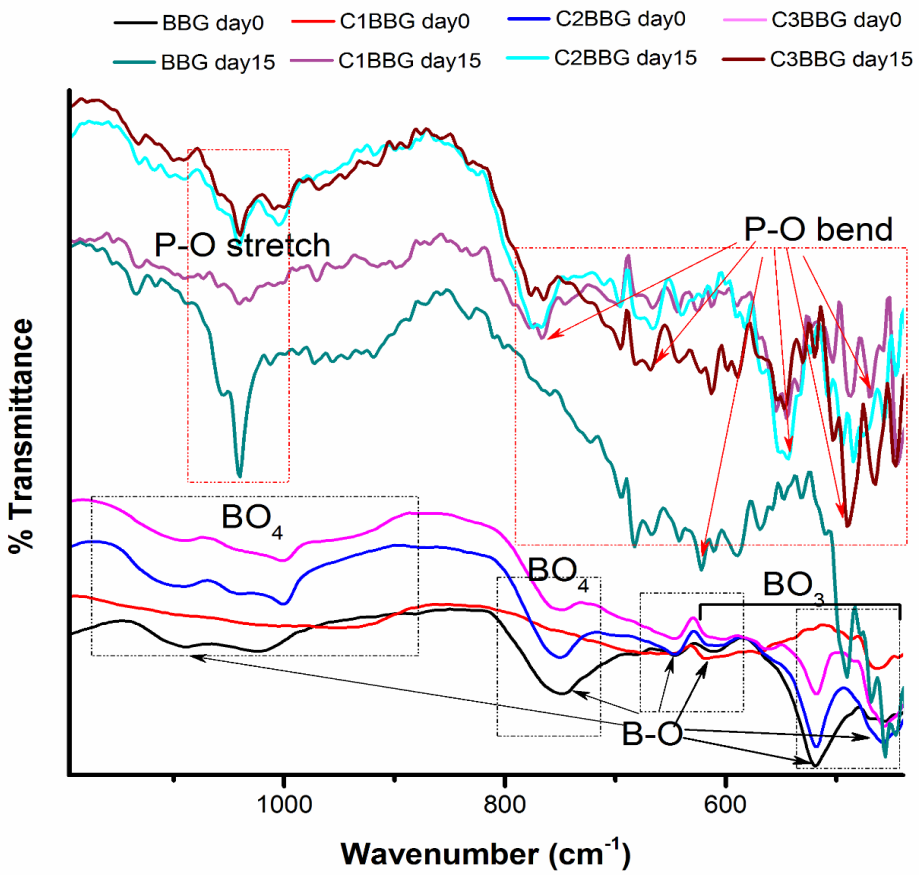

Fig 7.2 FTIR of BBGs showing characteristics resonances of HA formation due to soaking in SBF (above) comparing the untreated samples (below)

The effects of pH on formation of HA were studied. Further incorporation of copper into glass samples effecting the in vitro bioactivity were also assessed. Fig 7.3 reports variations in pH values of the glass samples in SBF solution depicting their HA formation ability. In this investigation the BBG was recorded with a sharp increase and maximum pH value (8.03; day15) compared to the rest scaffolds. However, C3BBG on day15 showed the least pH value (7.84) among all. The abrupt rise in pH was however observed up to day5 for the entire glass systems. The interesting finding by this pH investigation was their (1393B3 and their CuO derivatives) continuous and controlled increase in pH with number of days of immersion in SBF in contrast to silicate based 1393 glass systems.

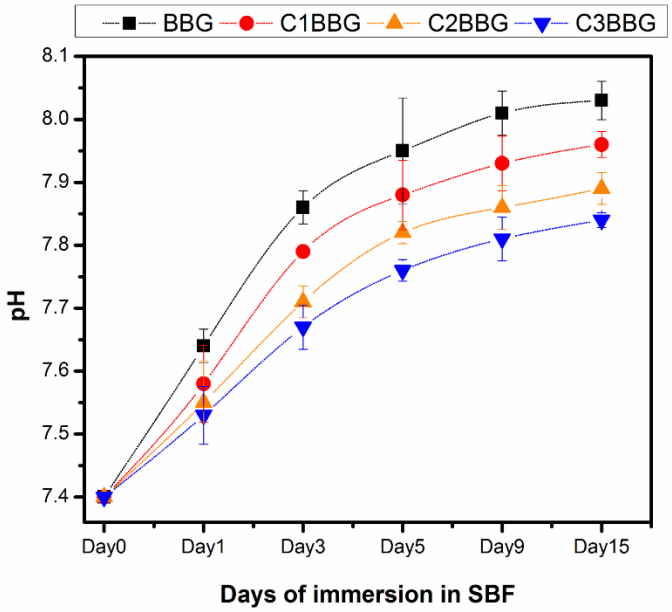

Fig 7.3 pH behavior as a function HCA layer formation upon immersion in SBF

Besides structural characterization, functional and chemical characterizations and morphological analysis are also very important in determining the in vitro bioactivity of bioactive glass samples. Fig 7.4 corresponds to morphological micrographs of the BBGs obtained from SEM-EDX analysis. Microscopic images of the scaffolds report needle/ rod alike nonhomogenous phases over the BBG and C1BBGs. However, the newly developed phases on C2BBG and C3BBG were more of like clusters of granules or elongated particles rather than rod-like morphologies. EDX analysis demonstrates the presence of elemental calcium and phosphate and other elements except for boron (because not being in an instrument's range boron was not detected in EDX).

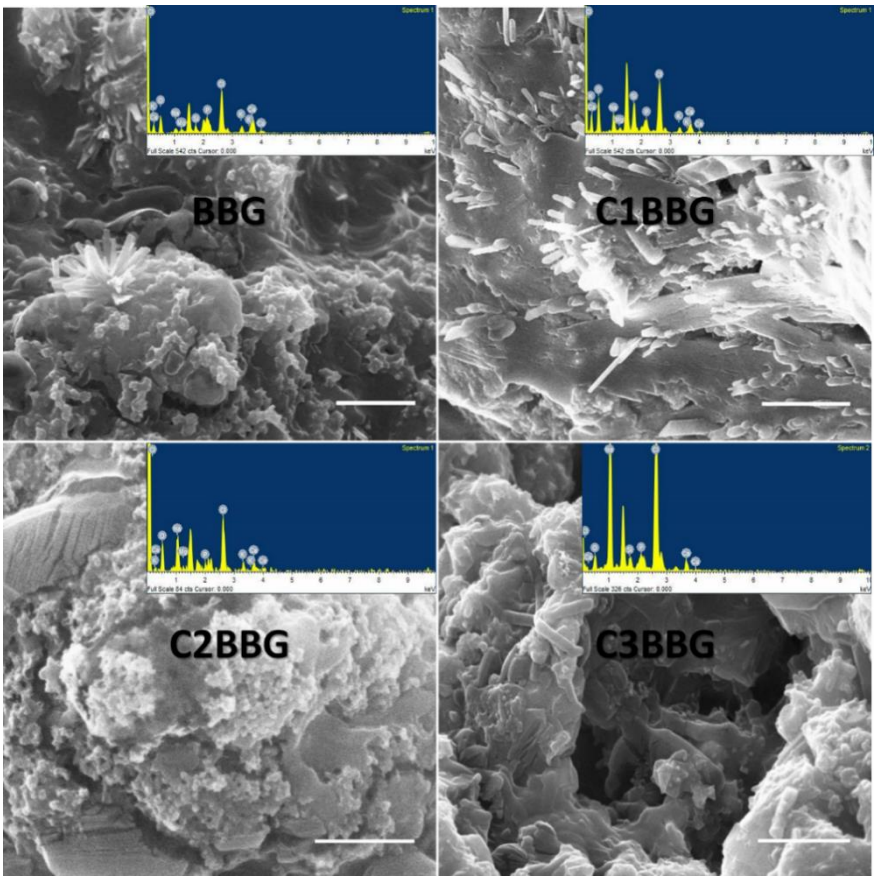

Fig 7.4 SEM and EDAX analysis of samples assessing surface modification due to HA formation. Inside bar=10µm.

7.4.2 Biological compatibility of L929 cells in BBGs

7.4.2.1 Cellular metabolism, viability and adhesion in scaffolds

Biological compatibility of BBG and CBBGs was examined by using L929 cell lines via metabolic activity, cell adhesion, and viability. The viability of cells in scaffolds was assessed through LIVE/DEAD assay, while metabolic activity and adhesion of cells on samples were detected through MTT assay and SEM analysis.

The results show that the maximum and minimum metabolic activity of L929 cells was observed respectively in C1BBG and C3BBG throughout the investigation, except in day1 (Fig 7.5). However, the cellular metabolism (absorbance at 570 nm) of L929 cell lines in BBG, C1BBG, C2BBG and C3BBG were 0.046 ± 0, 0.043 ± 0, 0.0487 ± 0, 0.04467 ± 5.7735E-4 (day1); 0.104 ± 0, 0.11433 ± 5.7735E-4, 0.069 ± 0, and 0.08667 ± 5.7735E-4 (day3); and 0.173 ± 3.39935E-17, 0.17623 ± 2.08167E-4, 0.13 ± 0, and 0.113 ± 0 (day7) respectively. The data clearly demonstrate that the cellular metabolic activity though insignificantly ($p \prec 0.05$), but most certainly enhanced after CuO incorporation into the parent glass system, except a few.

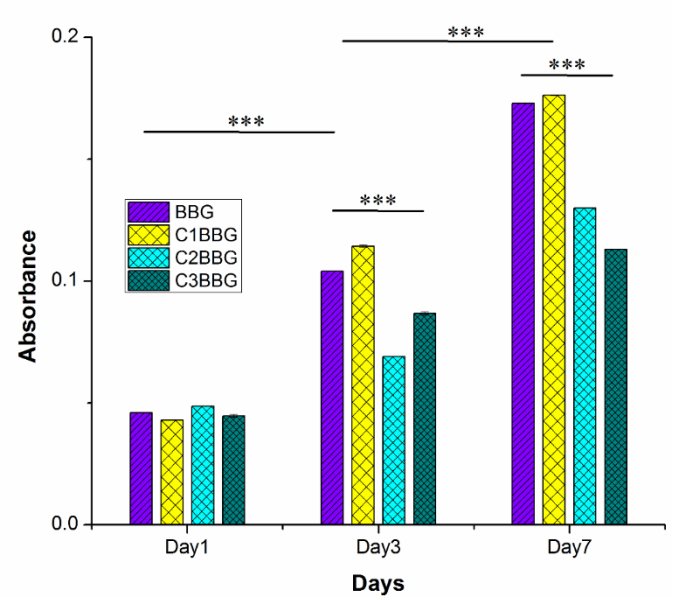

Fig 7.5 MTT showing cellular metabolic activity of L929 cells grown onto BBGs. Analysis of variance shows statistically significant changes in cellular metabolism. Data were considered significant (*) for p value <.05 and highly significant (**) for <.01 & p<.001 (n=3).

LIVE/DEAD assay (Fig 7.6) by Calcein AM and Ethidium homodimer-1 stain demonstrate viable (green) and dead (red) cells over the scaffolds. The retention of Calcein AM by live cells in the scaffolds was vividly noticeable by visual inspection. As per the visual inspection, the living cells were seemingly increased in the C1BBG and C2BBG in comparison to pure BBG. Moreover, the cellular viability was plausibly affected insignificantly, even up to 1 % CuO (C2BBG) incorporation into the glass system.

.

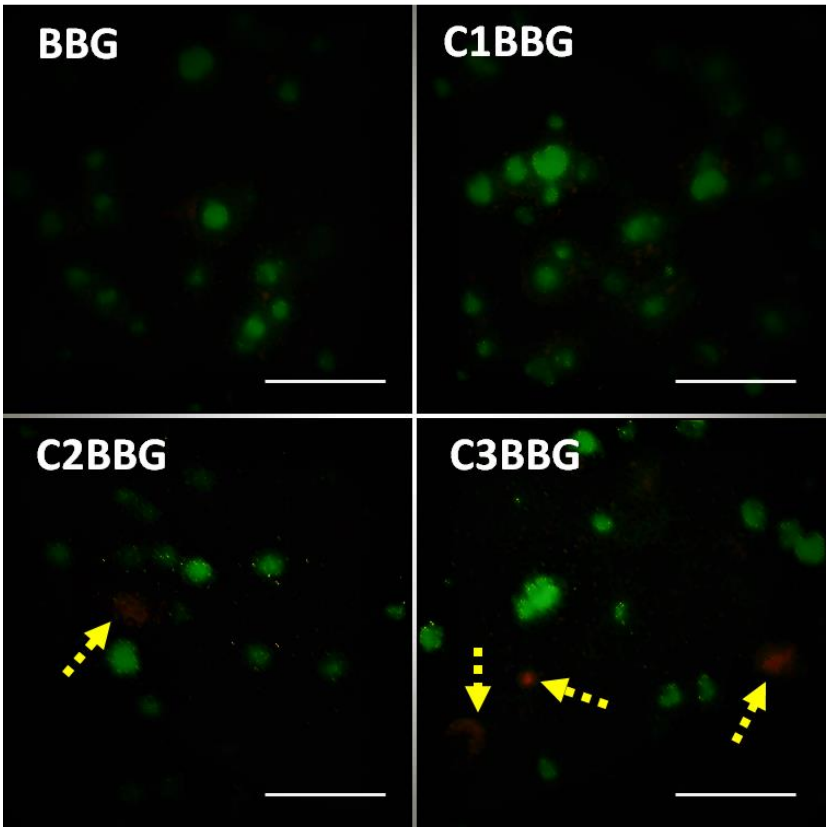

Fig 7.6 Live/Dead assay to assess cell viability of seeded onto the scaffolds. Fluoresced images showing Live (viable; green) and Dead (apoptotic; red) cells (inside bar =50 µm).

Cell attachments (Fig 7.7) onto the scaffolds' show analogous morphological demonstration over the entire sample sets. The elongated or irregular shaped cells were found adhering to the surface of the scaffolds. The cellular adhesion observed by the visual inspection looks augmented in CBBGs, except C3BBG. However, the cellular adhesion seemingly augmented the most in C1BBG in comparison to the other scaffolds.

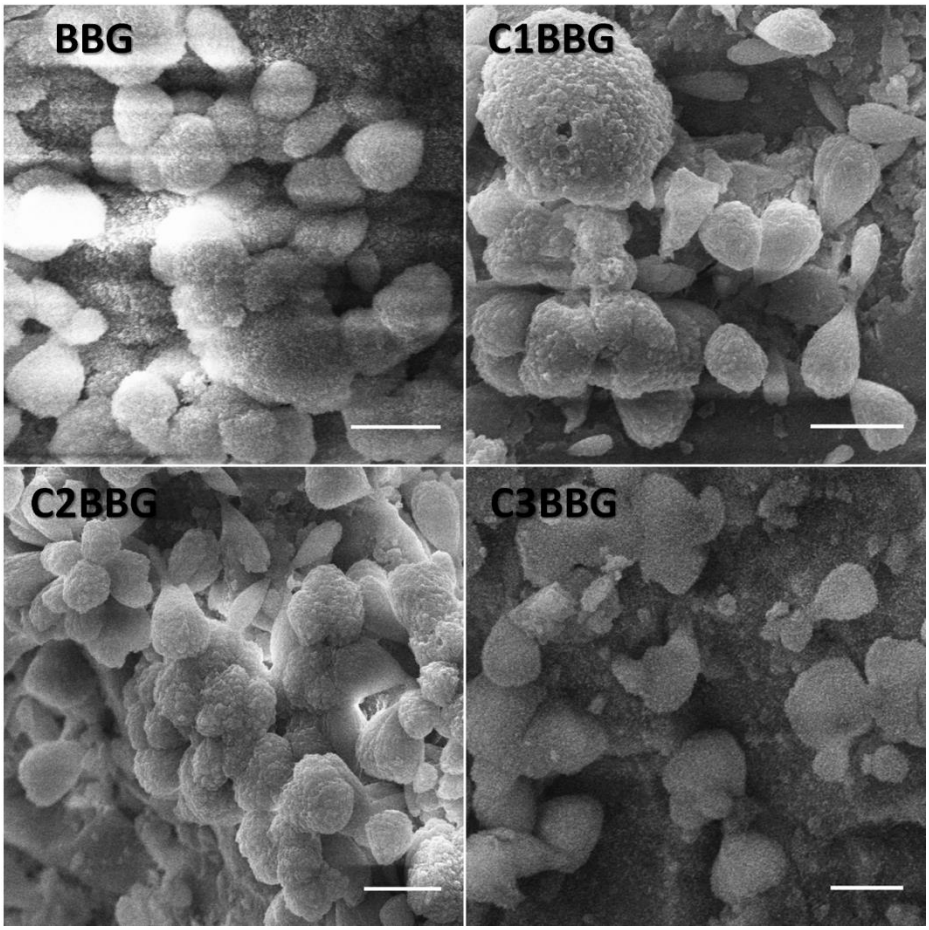

Fig 7.7 SEM micrographs of surface morphology of cell adhesion over scaffolds. The L929 (murine fibroblast cells) cultured for 24h over scaffolds appeared well adhered onto the scaffolds in almost all samples.

7.4.3 Physico-mechanical and physico-chemical properties of BBGs

The data reveal that the apparent porosity (due to the open pores) of scaffolds by the solvent saturation method was observed to be >50%. Microstructural analysis for pore geometry, pore size and pore size distribution (using NIH ImageJ software) also demonstrate that a nearly homogenous macroporous (>50 nm) scaffolds with pore size >100 μm pores (of about 99% pores) were formed. Moreover, the visible pore struts (indicated by yellow dashed arrow in Fig 7.8) in the scaffolds indicate their interconnectivity between pores.

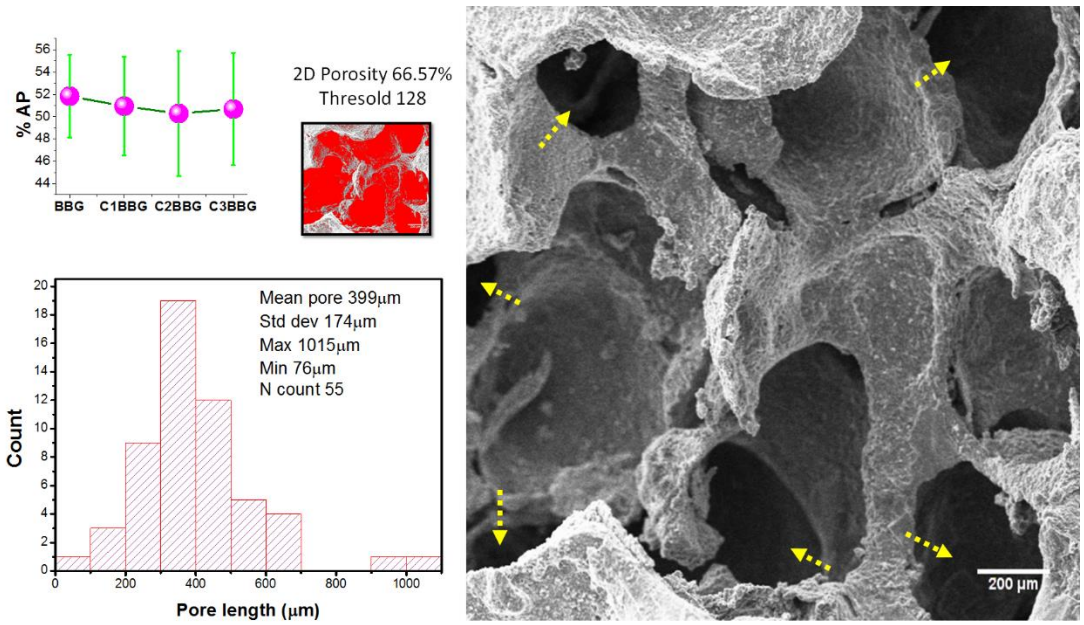

Fig 7.8 Physical property: Porosity (boiling water method, 2D porosity by NIH imageJ software) show the desired macroporous scaffolds were formed.

Nevertheless, the mechanical performances in CBBGs compared to pure BBG were found to be improved despite having similar pore profiles in all scaffolds. The compressive and bending properties of these porous scaffolds were recorded with an increase in values upon increasing CuO percentage into the glass system. However, the mechanical strengths

(compression; Fig 7.9 A and 3 point bending; Fig 7.9 B) of BBG, C1BBG, C2BBG and C3BBG were observed to be 9.96 ± 2.38 MPa, 7.8 ± 2.98 MPa, 11.64 ± 2.61 MPa, and 18.64 ± 2.44 MPa (compression) and 1.78 ± 0.37 MPa, 2.32 ± 0.39 MPa, 7.3 ± 0.192 MPa, and 9.1 ± 2.52 MPa (flexure). Further, the stress-strain curves (Fig 7.10) (in 3 point bend tests) determine the fracture behavior of the scaffolds. The linear behavior in stress-strain curves indicates the elasticity of the materials. It is important to mention that the peaks and valleys (zigzags) observed in the stress-strain curves were due to the bending, buckling, crumbling, and collapsing of porous struts under mechanical load. However, the zigzags in curves were lessened in CBBGs, implied that CuO addition had incorporated the metallic properties into the scaffolds. Bending moduli of elasticity equal to the tangent value (m=stress/strain) were derived from the approximately linear stress-strain curve (Fig 7.11) passing through the origin. The calculated values (flexural modulus) derived from stress-strain curves were found to be 144 MPa, 666 MPa, 731 MPa, and 1507 MPa for BBG, C1BBG, C2BBG, and C3BBG respectively. Modulus of toughness (energy absorbed per unit volume prior fracture; in Joules.meter^{-3}) of the samples was further measured by calculating (using integration gadget in Origin software at constant y baseline) the area under stress-strain curves. However, the calculated flexural toughness moduli were found to be 0.009, 0.01, 0.067 and 0.042 MPa (Newton/mm^2; stress) × mm/mm (i.e. unit less; strain) or 9000, 10000, 67000 and 42000 Joules.meter^{-3}.

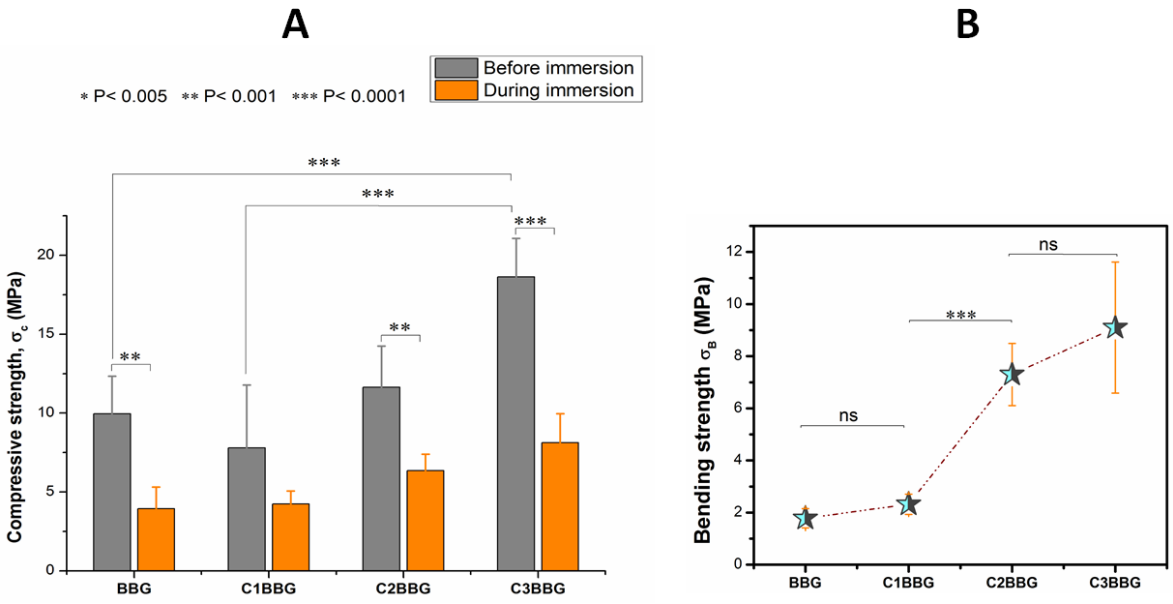

Fig 7.9 Mechanical properties: Compressive and flexural strengths of the BBGs were found enhanced upon CuO incorporation. Compression tests were performed in both dry and wet condition to validate their in vitro mechanical stability upon implantation. Statistical analysis considered significant changes for the p value <0.05; n=5.

Chemical durability or degradability of the scaffolds by means of weight loss was measured after immersion in SBF. The results report that the values (weight loss) were observed to be decreased with increasing CuO percentage in the parent scaffold system (Fig 7.11B).

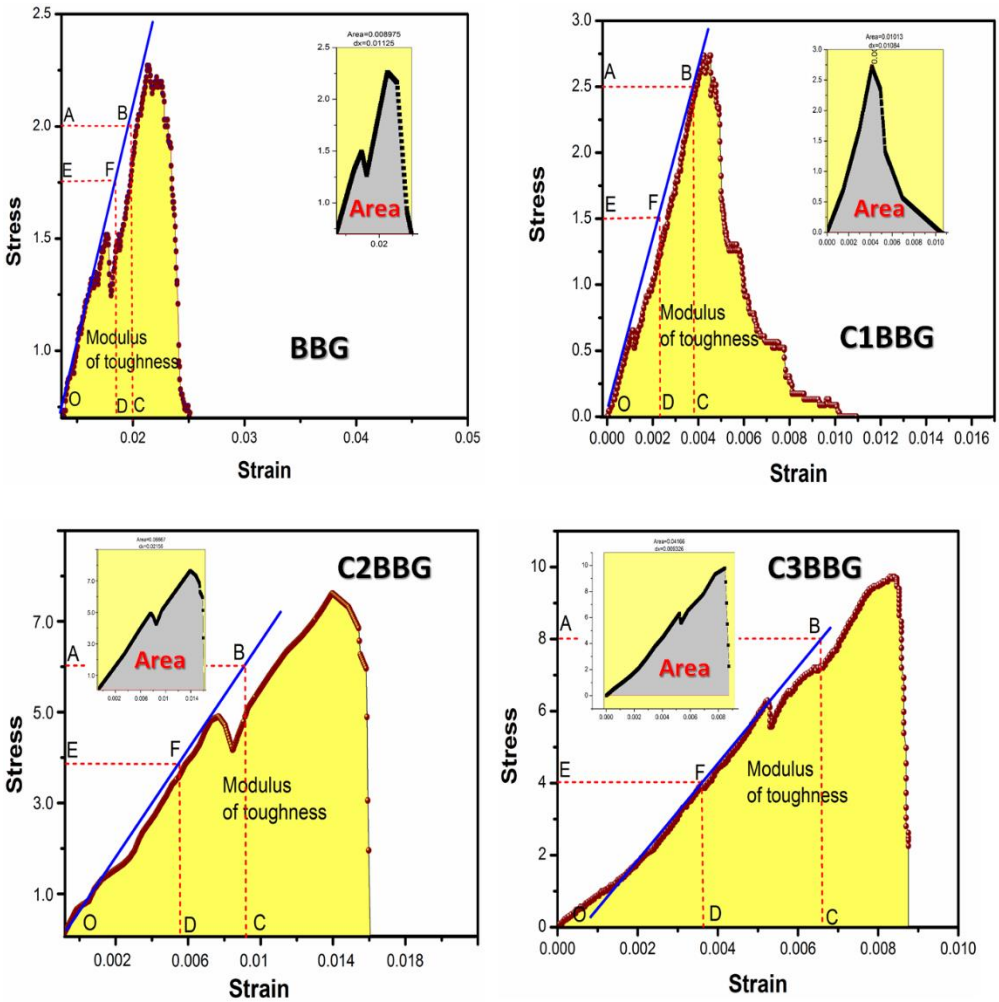

Fig 7.10 Stress-strain diagram of the BBGs confirm incorporation of elastic properties post CuO addition to the glass. Modulus of elasticity (details below) and modulus of toughness of the materials (area under curve) were found enhanced significantly after CuO incorporation into the glass.

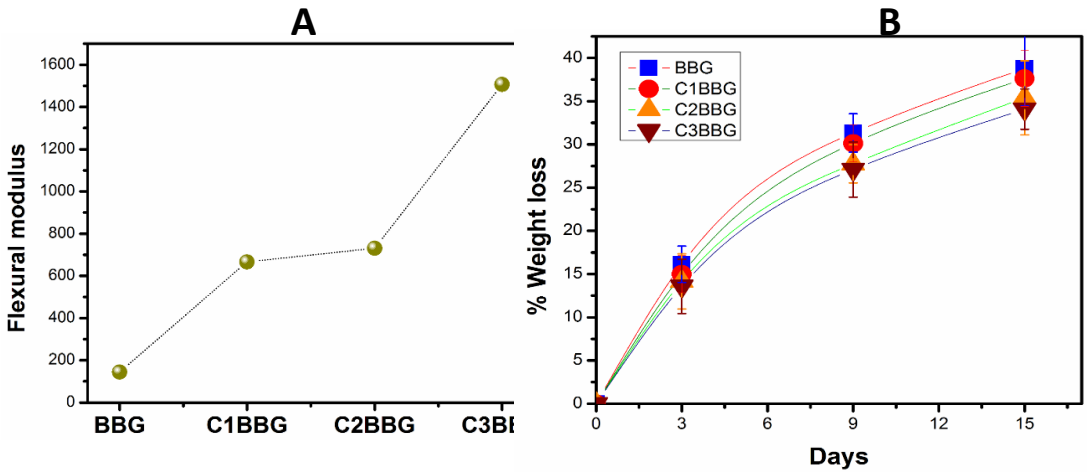

Fig 7.11 A. Flexural modulus calculated from stress-strain diagram **B.** Weight loss

7.4.4. The in vivo studies

7.4.4.1 Radiology

The day1 post-surgical radiographs of the bones demonstrate a considerable critical bone defects were created in femur bones of the animals (Fig Fig 7.12). The radiographs also demonstrate substantial healing of all bone defects after 35 days of surgery. However, the critical bone defects which were left untreated (Gr A-control) were seemingly less cured in comparison to the defects that treated with BBGs. Again, the visual observation of the bone defect radiograph demonstrates apparently better bone healing and remodeling for the defects treated with C2BBG than BBG.

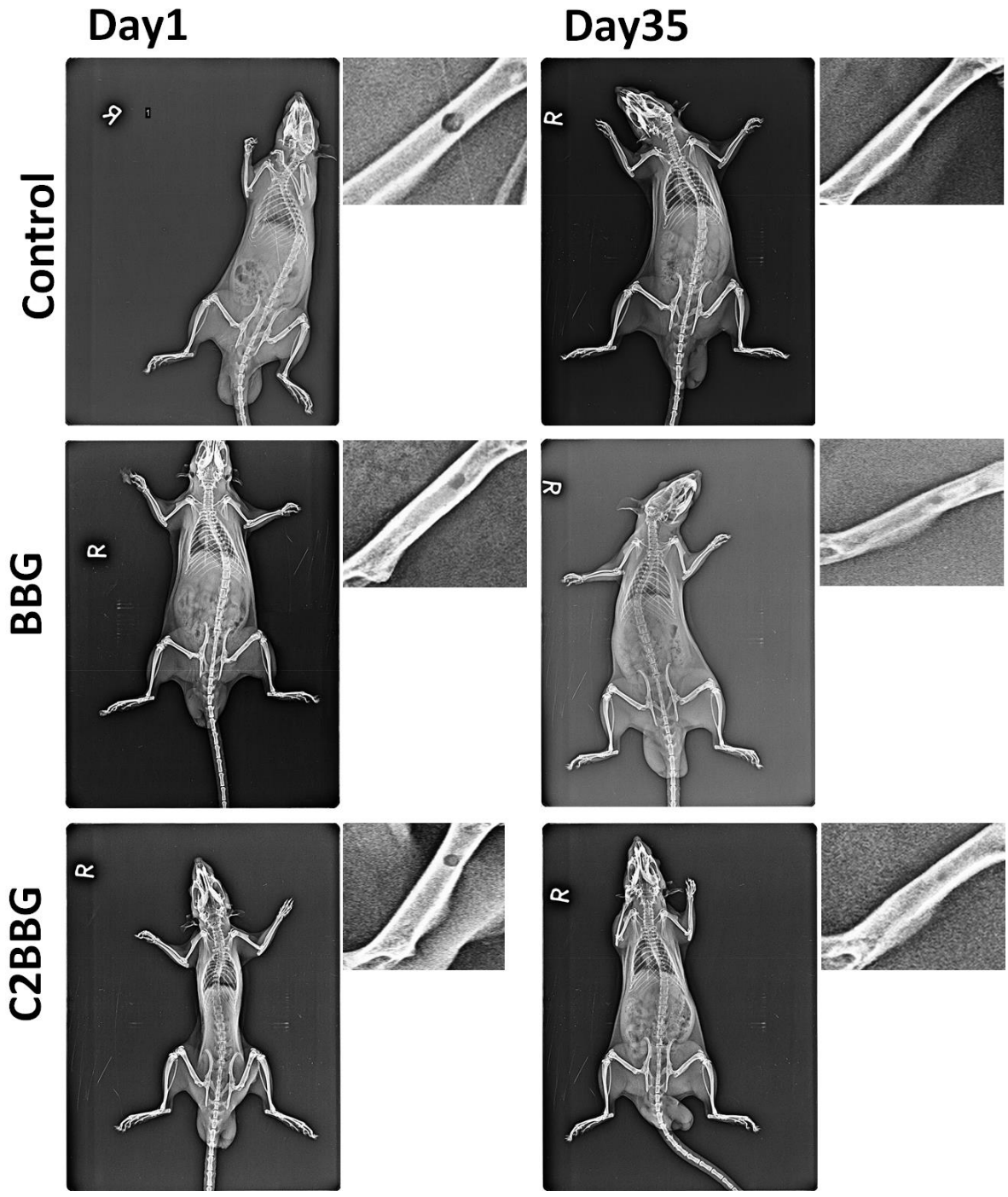

Fig 7.12 Radiography of bone defects of Wister-rats after 35 days of healing treated with materials (BBG, C2BBG) or without materials (Control)

7.4.4.2 Histology

Bone histology by H&E staining was performed to obtain better understanding of the bone formation morphology on the bone defect sites. H&E staining of the defected sites after 35 days of healing illustrates the osteogenic ability of the BBGs into bones in vivo (Fig Fig 7.13). A dense morphology of the specimen with osteoblasts was observed for the defects that has been filled with glass scaffold materials than that left untreated. Whereas, poor formation of fibrous connective tissues was seen at the defect sites of the control in comparison to the defects treated with BBGs. However, bone formation morphology in C2BBG seemed better as compared to BBG.

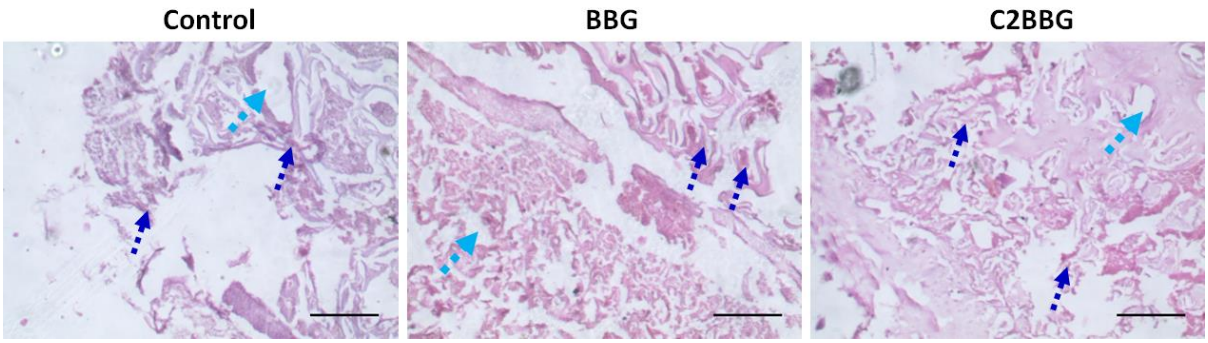

Fig 7.13 Histopathological examination of bone (femur bones) defects by H&E staining shows different osteogenic levels and bone regeneration ability of BBG, C2BBG and Control (devoid of material) at the defect sites. Blue arrow represents new bones and cyan arrow represents marrow space (inside bar =200 µm).

7.4.4.3 Analysis of biochemical parameters of blood serum

AST (aspartate aminotransferase) is an enzyme found inside liver cells. The higher amount of AST in the bloodstream is an indication of damaged liver. Likewise, the abnormal ALP (alkaline phosphatase) level in the bloodstream indicates of diseased liver, or and bones. Similarly, Creatinine and Urea are the two important biomarkers for kidney injury/disease.

Although the normal range of these enzymes in the blood serum of Wister rats is not very absolute, yet the lower the amount, the better. Some previous studies claimed that the normal limit of AST, ALP, and Creatinine to be 50-150 IU/L, 44-147 IU/L and 0.2-0.8mg/dL (Hasan et al., 2018). Whereas, in another research the serum ALP for control group (rats) was claimed to be ~400 IU/L.

However, in this investigation (Fig Fig 7.14), we observed the biochemical parameters within the normal range for all groups of animals. Moreover, biochemical markers of the blood serum study of the animals report C2BBG showed lower release of the biochemical enzymes than that of control and even BBG.

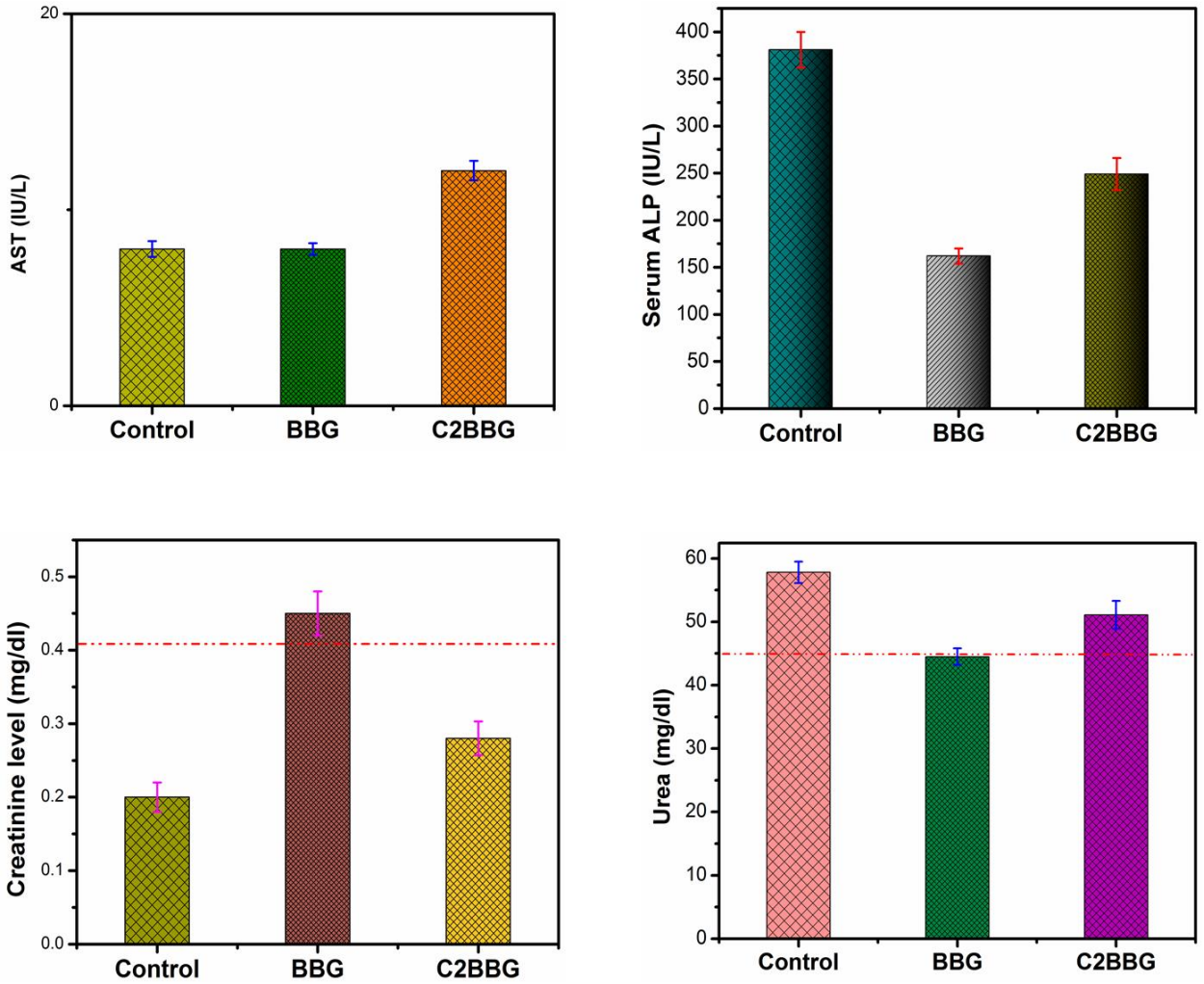

Fig 7.14 LFT (AST), RFT (Urea, Creatinine), and ALPase of blood assessing overall health (liver, kidney, and bone) of the animals post implantation (BBG, C2BBG).

7.5 Discussions

7.5.1 The in vitro bioactivity, mechanochemical and biological studies

X-ray diffractometry is one of the foremost characterization techniques through which bioactivity of materials is analyzed. Herein, the crystallographic changes of materials after immersion in SBF were examined to determine the bioactivity in vitro. The characteristic

changes in structural property report the bioactive nature of our derived scaffolds (BBG and CBBGs). Pronounced peaks at 2θ (angular value) 32˚, 45˚ and 56˚ were due to the appearance of HA crystals in soaked samples demonstrate that the samples are bioactive. The data were matched with standard ICDD data card (PDF number # 72-1243) in support of our statement. However, the other minor to moderate peaks were attributed to ulexite or boronatrocalcite ($CaNaB_5O_9$) [PDF number # 78-0294), henmilite ($Ca_2Cu[B(OH)_4]_2(OH)_4$) [PDF number # 40-0481] or calcium copper oxide(CCO; $CaCu_2O_3$ PDF number # 71-2295), calcium borate (CB; Ca $(BO_2)_2$ PDF number # 73-0804) and sodium borate (SB; Na_3BO_3 PDF number # 32-1047, $Na_2B_4O_7$ PDF number # 29-1179). Interestingly, the inclusion of copper into the glass system as observed in diffraction intensity of XRD spectra, caused no harm to the bioactivity of the materials. In fact, the pronounced peaks of CBBGs than BBG indicates their characteristic augmentation in bioactivity post CuO incorporation into the glass.

Characterizations of pH for bioactivity assessments were carried out through immersion of the samples in SBF for a particular period. Mineralization, the measure of bioactivity, has occurred through the SBF mediated heterogeneous nucleation and growth of critical-sized nuclei after accumulation of pre-existing (in solution) and leached out complexes from the glass surfaces. The ACP (amorphous calcium phosphates) converted into crystalline HCA (hydroxy-carbonated apatite) via OCP (octa-calcium phosphates) after accumulation of those species (Ca^{2+}, $PO_4{}^{3-}$and $CO_3{}^{2-}$) (Habraken et al., 2013, Yu et al., 2018). The rapid dissolution of ions increased the pH of the solution, which was, however, found steepest in BBG than those of CBBGs. The network structure of B_2O_3 could be responsible for higher pH of the SBF solution. Unlike SiO_4 tetrahedra, vitreous B_2O_3 occurs in the trigonal state

or hexagonal arrangements of $BO_{3/2}$ in boroxol ring. Although tetrahedral coordination can occur for crystalline B_2O_3, the building block ($BO_{3/2}$) of this network is two dimensional (planar) rather than 3-dimensional (3D) since the primary bonds exist within the plane (2D). However, the van der Waals bonds that exist in the third dimension are very weak; therefore, they could easily be disrupted. That is why T_g (glass transition temperature) and T_m (glass melting temperature) of borate glass is much lower (T_g-260 ˚C, T_m-450 ˚C) than the normal silicate glass. Moreover, since, the building block ($BO_{3/2}$) of the network is electron deficient (outermost orbit of $BO_{3/2,}$ filled with 6 electrons out of 8), the addition of ionic oxides (i.e., CuO) does not result in formation of NBO (non-bridging oxide) like silicate glass; instead, it gives rise to the network connectivity. The addition of ionic oxides converts the coordination of some of the borons from trigonal ($BO3_{/2}$) to tetragonal ($BO_{4/2}$), and henceforth, increase the connectivity of the network. Moreover, the CuO as network intermediate could have participated in glass network formation and enhanced the network connectivity. Also, the heat treatment might have increased the crystallinity of the CuO incorporated glasses. Thus, the CuO addition increasing connectivity and crystallinity of the glass would increase the bond strength, henceforth reducing borons' release. It is worth mentioning that the arguments are based on the related literatures only. However, further assurance need ion release studies. Wang et al. showed 99.7% release of B (Boron) in pure borosilicate (18% SiO_2, 36% B_2O_3) bioactive glass (BG) than that of 95.5% in BG-2Cu (2% CuO) in just 56 days (Wang et al., 2014). Nevertheless, the network forming elements (Boron) of 1393B3, unlike SiO_2 in 1393 bioactive glass, dissolute faster into the solution, resulted to the whole glass network become fragile. Therefore, the rapid conversion from glass to HA occurred. Also, the silica-rich layers that form on the silica based bioactive glasses in physiological fluid remains unconverted to an unknown period of time (Huang

et al., 2006, Yao et al., 2007, Fu et al., 2010), were most certainly not formed here on the BBGs.

In the FTIR results, the vibrational bands at 410-750 cm^{-1} and 1035 cm^{-1} were attributed to P-O bonds (Ali et al., 2018, Vyas et al., 2016, Ershad et al., 2017, Ershad et al., 2018, Yadav et al., 2017, Yadav et al., Ershad et al., 2020). The newly developed bands within the pre-existing B-O bands sometimes became pronounced due to their plausible superimposition (Krishnamacharyulu et al., 2016, Cui et al., 2017). Carbonyl hydroxyl bands (not shown) were observed at 1400-1800 and 2800-3800 cm^{-1}.

SEM micrographs exhibit needle or rod-like nonhomogenous phases or intermittent and dispersed hydroxyapatite particles on the glass surfaces. Moreover, elemental phosphate and calcium on the EDX spectrum reaffirm apatite layer formation for the SBF treated samples. The calculated Ca/P ratio from EDX data was also found comparable with the stoichiometric calcium to phosphate ratio of the bones (1.67). However, the surface morphology of the samples was found analogous for all the samples. Therefore, it can be concluded that the samples are all bioactive, and CuO addition did not harm to the bioactivity of the material.

Physical analysis reports a 51-56 % porosity with pore size greater than 100 µm (90% of the total pores) of the developed scaffolds. Characterizations of mechanical performance of those porous scaffolds revealed that the compression, flexure, elastic modulus, and toughness modulus of the scaffolds were largely influenced by CuO incorporation to the glass. Statistical analysis by one way ANOVA corresponds to significant improvements ($p<0.05$) in mechanical performance post CuO incorporation to the glass.

Although the mean compression value of C1BBG against the BBG decreased slightly and, of course, insignificantly, but the decrease in compression value was mainly due to the variations in their individual strengths. However, the improvement in compressive strength though statistically insignificant in C2BBG, but the enhancement was statistically significant ($p<0.05$) in C3BBG. However, the flexural strength, bending modulus, and toughness modulus of the scaffolds (CBBGs) were enhanced much in the CBBGs due to CuO incorporation.

Nevertheless, the flexural strengths were improved in all CBBGs compared to BBG, and the improvements were statistically significant ($p<0.05$) in both C2BBG and C3BBG and except C1BBG.

The increased linear stress-strain profile of CBBGs suggests enhanced elastic property in scaffolds due to incorporation of metallic property into the glass network.

The more linear stress-strain profile of CBBGs than BBG demonstrates that elastic property in scaffolds was incorporated into the glass post CuO addition. Elastic modulus of the glass materials was enhanced, and also brittleness was reduced (zigzags due to crumbling and crisping were reduced) by incorporating metallic properties after CuO incorporation to the parent glass system. Further, CuO addition to reinforcing the resultant glass and thereby increasing the toughness was also observed. Ceramics are known for their brittleness. Therefore, glass derived scaffolds are expected to show non-linear stress-strain profile due to fragile surface morphology. Combining metallic ions with glasses act as composite materials to reinforcement the structure, and thereby enhance the toughness and reduce brittleness, henceforth increase linearity in stress-strain curve. The enhancement in strengths of the bioactive glass scaffolds due to change in parameters, modification in

fabrication methodologies and metallic substitution was reported elsewhere (Fu et al., 2008, Ali et al., 2018, Ali et al., 2020b, Ali et al., 2020c, Ali et al., 2020a, Baino and Vitale-Brovarone, 2014).

Weight loss percentage as a measure of chemical durability was observed to be decreased with increasing CuO percentage. A maximum weight loss of 39 % was observed for BBG against the lowest (34 %) of C3BBG. Unlike our previous study (Ali et al., 2018), where CuO incorporation into silica based 1393 glass was seen weight loss increasing, the weight loss here in 1393B3 was, however, observed decreased upon increasing CuO percentage. The decreasing weight loss due to CuO incorporation can be used as controlling the degradability and release of the therapeutic ions (e.g., Cu). Thus, by the addition of CuO into 1393B3, the chemical durability was enhanced while degradability or conversion to HA was deferred.

The results report significantly improved ($p<0.05$) cellular metabolic activity in all the BBGs at day3 and day7 while compared with day1. However, the intragroup cellular metabolism (i.e., at fixed material concentration) was found to be more prominent in BBG and C1BBG than the C2BBG and C3BBG. Further, the differences in intragroup cellular metabolism, although insignificant at day1, but the changes were statistically significant at day3 and day7 (intragroup).

Also, an enhanced cellular metabolism was observed in C1BBG than pure BBG in day3 and day7. Cell adhesion study also reports similar results conforming to C1BBG and C2BBG were most compliant to cells (L929) than other BBGs. Microscopic images of cell adhesion demonstrate that the cells were found grown and attached better in C1BBG and C2BBG than BBG and C3BBG. The cellular viability and growth as ascertained by the

Calcein AM (green) retention in the living cells (L929) was appeared augmented in the BBG and C1BBG. However, the retention of Calcein AM seems comparable in C2BBG, but the dead cells (red; due to Ethidium homodimer stain) look plausibly increased in C3BBG than other BBGs.

7.5.2 The in vivo studies

The opacity of post-surgical radiographs demonstrate substantial healing of the bone defects for all group of animals. However, the bone regeneration for the animal treated with C2BBG seemed better than those treated with other BBGs, confirmed by a nearly radiopaque image of the radiological study. Moreover, noticeable black holes in the radiographs (due to radiolucency) in the control group and the BBG illustrate substantial defects after 35 days of bone healing compared to C2BBG, indicating lesser self-healing potential of control and BBG than C2BBG.

Bone healing study by Histopathological analysis (H&E staining) was also in conformity with the radiological examination. The prominence of fibrous connective tissues and osteoblasts cells in bone defects treated with C2BBG for 35 days suggests better bone healing ability of C2BBG than their counterparts.

Biochemical changes in relation to the health of the animals were also studied. The RFT, LFT, and other bone related biochemical enzymes (ALP) were observed to remain within the normal range in all animals. Nevertheless, the release of some biochemical enzymes in the bloodstream was found less in animals treated with C2BBG, as compared to others indicating their minimal effects on health, and thus better suitability. However, it is worth mentioning that there were zero intra- or post-operative deaths of animals throughout the

study. Further, the post-operative normal weight gain is an indication of good health for the animals.

7.6 Conclusions

The macroporous (pore dia >100μm; apparent porosity >50%) 1393B3 bioactive scaffolds (BBGs) were prepared and characterized through in vitro and in vivo investigations to analyze the mechanochemical and biological performance. The in vitro biological study demonstrate significant improvements in cellular viability and metabolism, minimal cell lysis, and a distinctive cellular attachments in the BBGs, particularly in C2BBG, compared to pure BBG. Also, the bone healing, evaluated through radiology and histology of bone, seems augmented again in the C2BBG than that of BBG and control. Moreover, the CuO incorporated scaffolds (CBBGs) exhibit significantly improved compressive and bending strengths than the pure BBG in most cases. Therefore, if taken altogether, the CBBGs, particularly C2BBG could be considered potential bone tissue regenerative materials upon further elucidations.